Increased SNR by Simultaneous Encoded Complex-Valued Slices with Through-Plane Acceleration in FMRI

Ke Xu[1] and Daniel B. Rowe[1,2]
[1] Department of Mathematical and Statistical Sciences, Marquette University, 1250 W Wisconsin Ave, Milwaukee, WI 53233
[2] Department of Biophysics, Medical College of Wisconsin, 8701 W Watertone Plank Rd, Milwaukee, WI 53226

Abstract
In functional Magnetic Resonance Imaging (fMRI), a topic of study is to accelerate the number of images per unit time to create each volume. Techniques have been developed such as Sensitivity Encoding (SENSE) and Generalized Autocalibrating Partially Parallel Acquisitions (GRAPPA) that measure less data in a slice (in-plane), but still are able to reconstruct an image. The simultaneous multi-slice (SMS) techniques provide an alternative reconstruction method in which multiple slices are acquired and aliased together concurrently (through-plane). Controlled Aliasing in Parallel Imaging (CAIPI) technique achieves slice-wise image shift to decrease the influence of the geometry factor (*g*-factor) of coil sensitivities. The Hadamard phase-encoding technique allows different combinations of the aliased slices and prevents the singular problem of the design matrix. In this paper, a CAIPI approach for multi-coil separation of parallel encoded complex-valued slices (mSPECS-CAIPI), a novel SMS approach is presented, combined with two slice-wise imaging shift techniques and Hadamard encoding method. The bootstrap sampling method and the least squares estimation function are also incorporated to calculate the reconstructed images. The signal-to-noise ratio (*SNR*) map and contrast-to-noise ratio (*CNR*) map are generated and compared with techniques without CAIPI shifts. An improvement of *SNR*, *CNR*, and activation values is achieved by the new approach.

Key Words: fMRI, through-plane acceleration, SMS, CAIPIRINHA, CAIPIVAT

1. Introduction

As a powerful tool, functional Magnetic Resonance Imaging (fMRI) has played a dominant role in Brain Imaging studies since 1990 when first discovered by Seiji Ogawa. Depending on the Blood Oxygen Level Dependent (BOLD) contrast signal, the Magnetic Resonance Imaging (MRI) machine can map the brain and demonstrate the spatial and temporal changes in brain metabolism (Glover GH, 2011; Ogawa et al., 1990). In structural and functional MRI studies, the time to measure a volume image is dependent upon how rapidly the necessary amount of data needed to reconstruct an image can be measured. In order to accelerate the number of images measured per unit time, a topic of study has been to measure less data but still be able to reconstruct a high-quality image. In order to reconstruct images using less data, multiple receiver coils are used where each coil measures sensitivity-weighted images. Initially, accelerated imaging was aimed at In-Plane Acceleration (IPA) where lines of spatial frequency data are skipped, and each coil measured less lines of spatial frequency. In Parallel Imaging techniques, like Sensitivity Encoding (SENSE) and Generalized Autocalibrating Partially Parallel Acquisitions (GRAPPA) (Griswold et al., 2002; Pruessmann et al., 1999; Sodickson and Manning, 1997), a single slice has been excited, and partial lines of *k*-space skipped, resulting in a sensitivity weighted aliased image for each coil, that is combined into a single complete image. However, considering some fixed time blocks in the data-acquiring process, for

instance, imaging encoding and the proper time for T_2^* contrast in one excitation, the scan time will not decrease significantly in parallel imaging technique. More recently, Simultaneous Multi-Slices (SMS) techniques were developed and discussed (Barth et al., 2016; Souza et al., 1988). The SMS technique is widely used in fMRI studies, and it allows for acquiring fMRI data with high resolution by using a multiband radiofrequency (RF) within a reduced repetition time (TR). Compared with conventional parallel imaging techniques, in SMS techniques, multiple slices are acquired concurrently and aliased together in one excitation, and hence, the image-acquiring time will decrease with a factor of the total number of aliased slices. Thus, a Through-Plane Acceleration (TPA) is achieved by SMS techniques and allows for a more efficient approach to acquiring images. In this paper, a novel SMS imaging reconstruction technique with high acceleration factor, a Controlled Aliasing In Parallel Imaging approach for multi-coil Separation of Parallel Encoded Complex-valued Slices (mSPECS-CAIPI), will be presented and discussed.

Since multiple slices are acquired at the same time for one excitation of the TPA technique, a short distance between aliased slices will lead to a high similarity of coil sensitivity information. When applying the standard SENSE method, this will easily cause a singular matrix problem and strong inter-slice signal leakage will appear on the reconstructed images. In order to decrease the influence of the geometry properties of the coil sensitivity maps, techniques like "controlled aliasing in parallel imaging results in higher acceleration" (CAIPIRINHA) and "blipped-CAIPIRINHA" (Blipped-CAIPI) provide other possible ways to minimize the influence of the geometry factor (*g*-factor) and increase the rank of the slices aliasing matrix (Felix et al., 2005; Setsompop et al., 2012). By modulating the phase for each line in the *k*-space and imparting each line with a specific angle, the field-of-view (FOV) will be moved in the phase encoding direction (PE). Applying a unique phase modulation amount to each slice in the aliased image-acquiring process, the physical distance among the aliased voxels will increase. Therefore, the independence of coil sensitivity for each slice will increase and the influence of the *g*-factor for each excitation will be minimized. Moreover, to further increase the physical distance between two aliased voxels and expose more information beneath the coil sensitivities, FOV can not only be moved along the PE direction but also the readout direction (RO). The study "multislice CAPIPRINHA using view angle tilting technique" (CAIPIVAT) (Jungmann et al., 2015; Min-Oh Kim et al., 2016) proposes a method combining the CAIPIRINHA technique and View Angle Tilting (VAT) (Min-Oh Kim et al., 2012) technique together by applying a unique compensation gradient of VAT. Other techniques to solve the singular matrix problem of the design matrix, like the "simultaneous multi-slice acquisition" (SIMA) (Souza et al., 1988) method discussed a powerful tool, the Hadamard phased-encoding technique in the reconstruction process. By incorporating a specific coefficient from the Hadamard matrix for each aliasing slice, different combinations for each voxel will be achieved. For example, the summation of two desired voxels will not only be acquired but also the difference between two voxels will be collected. In the "Separation of parallel encoded complex-valued slices (SPECS) from a single complex-valued aliased coil image" and "multi-coil separation of parallel encoded complex-valued slices" (mSPECS) studies, Hadamard phase encoding technique is also the essential idea (Kociuba CM 2016; Rowe et al., 2016). The SPECS technique and the mSPECS technique are critical milestones of this study. SPECS presents a method that combines the Hadamard phase encoding technique and the CAIPIRINHA together with one single coil. However, mSPECS presents a method with the Hadamard phase encoding technique and multiple coils without any slice-wise image shift.

In the mSPECS-CAIPI model, we incorporate image shift techniques and the Hadamard phase-encoding technique together, different voxel combinations will be acquired for each excitation. In the unaliasing process, calibration reference images will be artificially aliased, and the artificial aliasing matrix will be used to form a regularizer in the separation process. The bootstrap sampling approach is also incorporated into the model to eliminate the inter-slice signal leakage in the reconstruction images at the cost of a slightly increased variance of the calibration images forming the regularizer. The least squares estimation technique is applied in this model to calculate the estimation reconstruction voxel values. The mSPECS-CAIPI model provides a solution to significantly reduce the scan time with a high acceleration factor, meanwhile providing high-

resolution and high-quality reconstruction images. Moreover, the mSPECS-CAIPI model is a solid step for future research which further increased the acceleration factor with IPA and TPA together.

2. Theory

In this section, the mSPECS-CAIPI model will be illustrated in three subsections. First, the data-acquiring process will be presented including unique slice-wise image shift methods, CAIPIRINHA and CAIPIVAT, and the Hadamard phase encoding technique. The image aliasing process will be discussed in detail in this section. Second, the artificial aliasing of the calibration images process will be presented to improve the condition of the design matrix. Third, a statistical separation process will be presented. The mechanism of reducing the inter-slice signal leakage will be explained in this section.

2.1 The Data Acquiring Process

2.1.1 The CAIPIRINHA and the CAIPIVAT

Due to the high similarity of coil sensitivities between two short-distance aliased slices, diminishing the influence of the *g*-factor will be the main consideration in the SMS study. The "controlled aliasing in parallel imaging results in higher acceleration" (CAIPIRINHA) method proposes a way to reduce the dependence on the geometry of the coil array by increasing the distance between aliased voxels on the phase-encoding (PE) direction. This is accomplished by modulating the phase for each line in *k*-space. The "blipped-CAIPIRINHA" (Blipped-CAIPI) technique extends the methodology of CAIPIRINHA and adjusts the phase modulation amount in *k*-space to eliminate the voxel blurring/tilting effect. Moreover, the independence of sensitivity information for each coil will increase by applying the slice-wise shifts. The "multislice CAIPIRINHA using view angle tilting technique" (CAIPIVAT) proposes a method combining the CAIPIRINHA technique and the View Angle Tilting (VAT) technique together. Similar to the CAIPIRINHA technique and the blipped-CAIPIRINHA technique, the CAIPIVAT model shifts the field-of-view (FOV) along the PE direction. Meanwhile, slice-wise shifts along the readout (RO) direction will be achieved by applying a unique compensation gradient of VAT. Thus, the distance between aliased voxels will further increase. In this project, we implement the principal idea of the blipped-CAIPI technique and the CAIPIRINHA technique with the Hadamard phase encoding method to improve the image reconstruction process. We will also combine the CAIPIVAT technique and the Hadamard phase encoding method together, and the performance of this approach will be investigated.

According to the definition of the signal-to-noise ratio (*SNR*) (Welvaert and Rosseel, 2013), in the SMS studies, the *SNR* ratio is given by:

$$SNR_{SMS} = \frac{SNR}{g\sqrt{R}}. \tag{2.1}$$

From the Eq. 2.1, the SNR_{SMS} is strongly influenced by the geometry properties of coil array, *g*-factor. It depends on the number and location of the coils, the phase-encoding direction, the voxel location, etc. Thus, the *g*-factor is not a constant number but varies across each voxel within the images (Preibisch et al., 2015). The short physical distance between two aliased voxels will increase the *g*-factor value because of their intensity and sensitivity similarity which will decrease the *SNR* ratio. Therefore, increasing the physical distance between two aliased voxels is one of our strategies. The CAIPIRINHA technique can reduce the influence of the *g*-factor by applying a partial in-plane image shift. Considering the 1D inverse discrete Fourier transform, a periodic time series $y(t)$ sampled at n time points Δt apart is described as below:

$$y(p\Delta t) = \sum_{q=-\frac{n}{2}}^{\frac{n}{2}-1} f(q\Delta v) e^{i\frac{2\pi}{n}pq} \quad for\ p = 1, \dots, n \tag{2.2}$$

where Δv is the temporal frequency resolution and $\Delta v = \frac{1}{n\Delta t}$. It is the summation of the Fourier amplitude coefficients at multiple various frequencies. In Eq. 2.2, $y(p\Delta t)$ and $f(q\Delta v)$ are complex-valued quantities with real and imaginary components. When we shift the whole time series from

$p\Delta t$ to $p'\Delta t$, where $y(p'\Delta t)$ is same as $y(p\Delta t)$ sampled at n time points Δt apart with a different order from $y(p\Delta t)$, a field-of-view shift Δy will happen and is calculated as:

$$\begin{aligned}\Delta y &= y\big((p-p')\Delta t\big)\\ &= \sum_{q=-\frac{n}{2}}^{\frac{n}{2}-1} f(q\Delta v)\, e^{i\frac{2\pi}{n}(p-p')q}\\ &= \sum_{q=-\frac{n}{2}}^{\frac{n}{2}-1} f(q\Delta v)\, e^{i\frac{2\pi}{n}pq} e^{-i\frac{2\pi}{n}p'q} \quad for\ p = 1, \dots n\end{aligned}$$

The FOV shift only depends on the phase change in *k*-space, which equals $-\frac{2\pi}{n}p'q$. If $p' = 1$, which means the image moves one voxel distance in the PE direction, the modulation quantity of phase will be $-\frac{2\pi}{n}q$. If half of the image will be moved in the PE direction (FOV/2), $p' = \frac{n}{2}$, the modulation of phase should be $-\pi q$. Therefore, the phase of even lines in *k*-space should impart $\pi/2$ and the phase of odd lines should impart $-\pi/2$. If the FOV/4 shift of the image needs to be achieved, the modulation of the phase for each line in the *k*-space needs to be adjusted. Figure 2.1 is an illustration to explain the CAIPIRINHA process. Applying discrete Fourier transform to each excitation in the time series to get the *k*-space, modulating the phase for each line in the *k*-space with a unique angle, after the inverse discrete Fourier transform, we will have an in-plane image shifted effect. Compared with the on-resonance spins of the CAIPIRINHA technique, during the slice-selection process, the CAIPIVAT technique allows off-resonance spins at different locations. The VAT technique projects the excited spins along a unique view angle to map the brain with a specific spatial shift on the image plane. Figure 2.2 is an illustration to explain the CAIPIVAT process. After the Fourier transform to acquire the *k*-space of the original image, the CAIPIRINHA technique is applied to the k-space of each slice. A global phase modulation will be added to each slice at the same time.

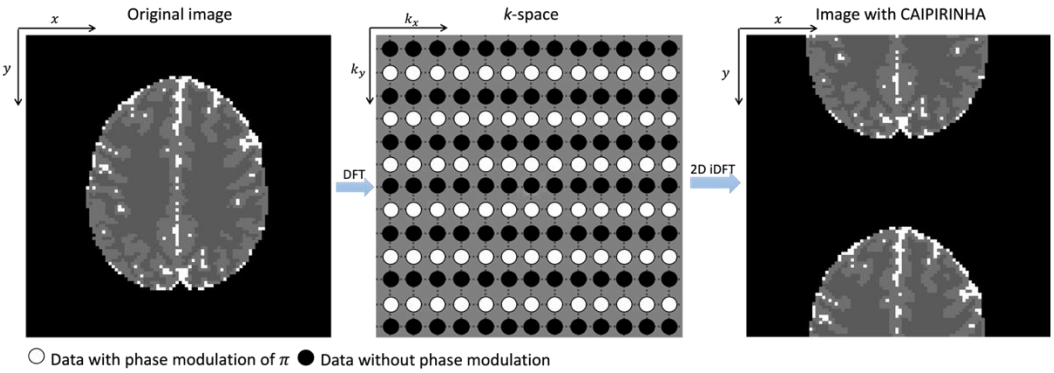

Figure 2.1. An illustration of the CAIPIRINHA process. The image on the left is one slice of a simulated brain image. After the discrete Fourier transform and modulating the phase with a unique value for each line in the *k*-space, images with unique FOV shifts along the PE direction (vertical) will be acquired after the inverse discrete Fourier transform.

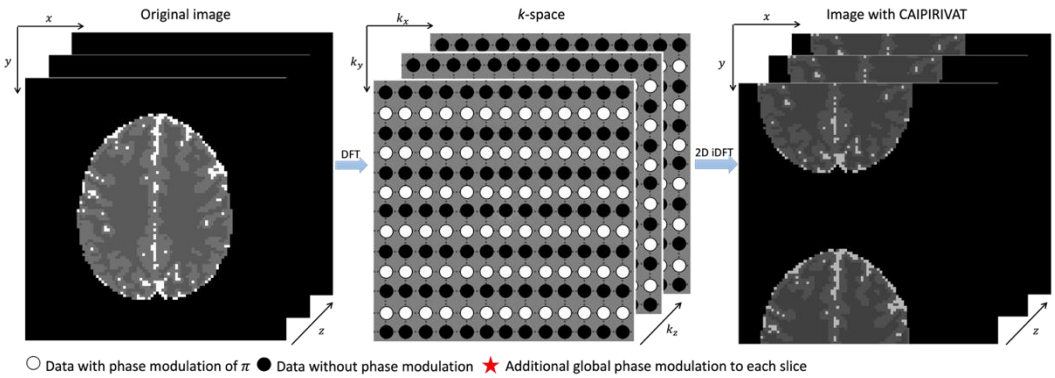

Figure 2.2. An illustration of the CAIPIVAT process. The image on the left is one slice of a simulated brain image. After the discrete Fourier transform and modulating the phase with a unique value for each line in the *k*-space, a global phase modulation will be added to each slice. Images with unique FOV shifts along the PE direction (vertical) and the RO direction (horizontal) will be acquired after the inverse discrete Fourier transform.

In this study, the principal idea of the CAIPIRINHA technique and the blipped-CAIPI technique will be applied first. For each slice within each excitation, we imply $\Delta y = (l-1)FOV/N_s$ in-plane image shift, where $l = 1, \dots, N_s$ and N_s is the total number of aliased slices. On the TR dimension, we also imply the CAIPIRINHA technique for each excitation by $\Delta y = (m-1)FOV/N_s$ in-plane image shift, where $m = 1, \dots, N_s$ and N_s is the total number of aliased slices. Thus, with the in- and through-excitation image shift, at $TR = N_s + 1$ excitation time point, the aliased artifacts should be the same as the $TR = 1$ excitation time point. In Figure 2.3, on the left is an example of an in- and through-excitation image shifts process with $N_s = 4$ incorporating with the CAIPIRINHA technique. When $TR = 5$, the image shift pattern for each slice should be the same as the time point $TR = 1$. Furthermore, the principal idea of the CAIPIVAT technique will also be applied. Similar to the CAIPIRINHA technique, $\Delta y = (l-1)FOV/N_s$ for the in-plane image shift and by $\Delta y = (m-1)FOV/N_s$ for the through-plane image shift will be applied to each excitation along the phase-encoding direction. For each slice within each excitation, a unique image shift will appear horizontally on the RO direction with the support of the CAIPIVAT technique. The shift distance for each slice along the RO direction can be calculated and depend on the distance between the desired aliased slices, the compensation gradient, and the RO gradient. A modest slice-wise shift will be applied for each excitation to ensure the brain image is not outside the FOV. In Figure 2.3, on the right is an example of in- and through-excitation image shift process of $N_s = 4$ incorporating with the CAIPIVAT technique. Besides the same amount of the FOV shift in- and through-excitation on the PE direction as CAIPIRINHA technique, slice 1 and slice 3 will have a FOV shift to the left as well as slice 2 and slice 4 will have a FOV shift to the right on the RO direction according to the CAIPIVAT technique. Thus, comparing with the CAIPIRINHA technique approach, the overlapping area between two desired aliased images will decrease and the independency of the sensitivity for each coil will increase. Moreover, based on the sequential properties, the image shift pattern for each slice should be the same as the time point $TR = 1$ when $TR = 5$.

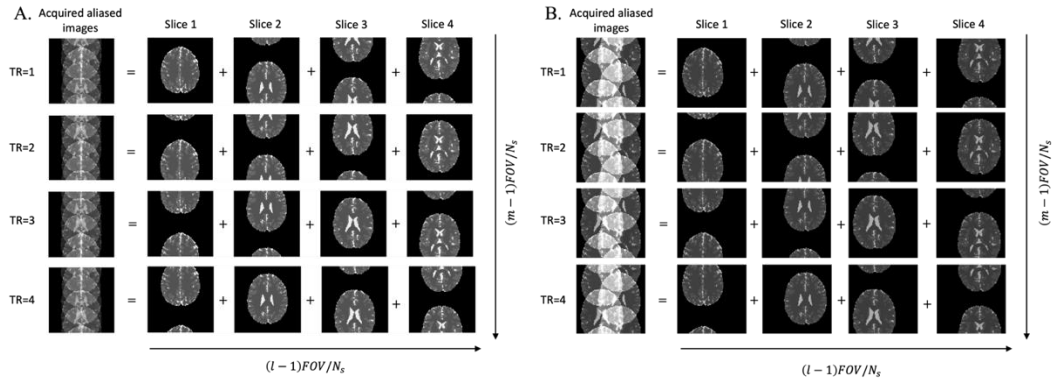

Figure 2.3. A. An example of in- and through-excitation image shift process with $N_s = 4$ by applying the CAIPIRINHA technique. On the in-excitation direction, $(l-1)FOV/N_s$ was applied for each slice where $l = 1, \dots, N_s$. On the through-excitation direction, $(m-1)FOV/N_s$ was applied for each excitation where $m = 1, \dots, N_s$. B. An example of in- and through-excitation image shift process with $N_s = 4$ by applying the CAIPIVAT technique. On the in-excitation direction, $(l-1)FOV/N_s$ was applied for each slice where $l = 1, \dots, N_s$. On the through-excitation direction, $(m-1)FOV/N_s$ was applied for each excitation where $m = 1, \dots, N_s$. For each excitation, slices 1 and slice 3 will slightly shift to the left on the RO direction, whereas slice 2 and slice 4 will shift to the right on the RO direction according to the CAIPIVAT technique.

2.1.2 The Hadamard Phase Encoding

The Hadamard encoding technique is a well-developed volume excitation method. The conventional magnetic resonance (MR) imaging techniques have been limited by the size of the matrix for the acquired aliased images. The Hadamard phase-encoding method allows the increment of the size of the acquired aliased image matrix by aliasing in both frequency and phase encoding dimensions. With the support of this simultaneous binary-encoded technique, the TR will decrease, and the SNR ratio will improve. The Hadamard matrix is given by:

$$H_{2^n} = \begin{bmatrix} H_{2^{n-1}} & H_{2^{n-1}} \\ H_{2^{n-1}} & -H_{2^{n-1}} \end{bmatrix} = H_2 \otimes H_{2^{n-1}} \tag{2.3}$$

$$H_1 = [1], H_2 = \begin{bmatrix} 1 & 1 \\ 1 & -1 \end{bmatrix}$$

where $\otimes$ denotes the Kronecker product. It is a square matrix with elements of either +1 or -1. In the mSPECS-CAIPI study, each excitation is sequentially coordinated with a unique Hadamard aliasing pattern. To improve the computational efficiency, we manually assign the size of the Hadamard phase-encoding matrix to be the same as the number of the aliased slices. Thus, the size of the Hadamard phase-encoding matrix is $N_s \times N_s$, N_s denotes the total number of aliased slices in one TR. In this aim, $H_{\delta,z}$ is the δth row and zth column element of Hadamard matrix corresponding to sth slice in δth TR. Same as the sequential properties of image shifts, the Hadamard phase-encoding aliasing pattern will cycle through along the TR dimension. For example, the Hadamard aliasing pattern of $TR = N_s + 1$ should be the same as $TR = 1$. Figure 2.4 is an example of the Hadamard aliasing pattern when $N_s = 4$. In Figure 2.3, a) is a 4×4 Hadamard matrix, b) is the Hadamard coefficients for each slice in the fMRI time series, c) is the phantom brain images multiplied by Hadamard aliasing coefficients at the first 4 TRs. In order to increase the distance between two aliased voxels and reduce the influence of the g-factor, we introduce the term "packet" to indicate the slice aliasing circumstance. For example, under a circumstance with $N_s = 8$, we put odd number slices into one packet (i.e., slice 1, slice 3, slice 5, and slice 7), and even number slices into another packet (i.e., slice 2, slice 4, slice 6, and slice 8). Therefore, we will have 2 packets in this situation, and both packets will coordinate with the same Hadamard phase-encoding aliasing pattern. With the help of the packet technique, the slice-to-slice signal leakage artifacts will diminish.

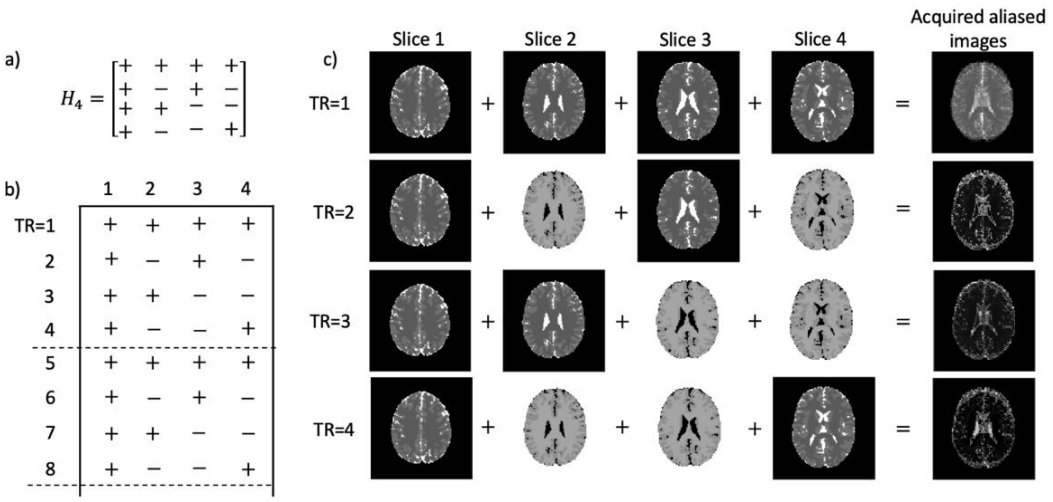

Figure 2.4. An illustration of Hadamard phase-encoding aliasing pattern when $N_s = 4$. (a) is the H_4 matrix with plus sign denotes as 1 and minus sign demotes as -1. (b) is sequential Hadamard aliasing coefficient for each slice in the fMRI time series. (c) shows the phantom brain images multiple Hadamard aliasing coefficients at the first 4 TRs.

2.1.3 A Single Aliased Voxel

Given a single aliased voxel, $a_{j,\gamma,\delta}$, at the location (x, y) of aliased images, with δth Hadamard aliasing pattern and γth matrix rotation operation, measured at coil j, is defined as the summation equation:

$$a_{j,\gamma,\delta} = \sum_{z=1}^{N_S} H_{\delta,z} R_{\gamma,z} S_{j,z} \beta_z + \varepsilon_j \tag{2.4}$$

In Eq. 2.4, $a_{j,\gamma,\delta}$ is a 2×1 complex-valued vector with the real and imaginary components of the acquired aliased voxel value measured at coil j, with rotating operation γ and Hadamard phase-encoding aliasing pattern δ. The Hadamard phase-encoding aliasing pattern, $H_{\delta,z}$, is the same as the definition in section 2.1.2. Hadamard Encoding, where parameter δ corresponds to the order of Hadamard coefficients pattern, and parameter z corresponds to the number of slices. The coefficients of $H_{\delta,z}$ will be either +1 or -1. The matrix rotation operator, $R_{\gamma,z}$, is closely related to the definition of section 2.1.1. Subscript γ denotes the order of the matrix rotation operation for each TR, and parameter z corresponds to the number of slices. The coil sensitivity matrix, $S_{j,z}$, is a 2×2 skew symmetric matrix with the real and imaginary components at coil j for slice z, $S_{j,z} = [S_R, -S_I; S_I, S_R]_{j,z}$. The true voxel value, β_z, is a 2×1 complex-value vector with the real and imaginary parts of the aliased voxel in slice z. The measurement noise, ε_j, is also a 2×1 complex-value vector with real and imaginary parts. The mean of measurement noise is $E(\varepsilon_j) = 0$, and the covariance of error is $cov(\varepsilon_j) = \sigma^2 I_2$, where I_2 is a 2×2 identity matrix. There is no correlation between the real and imaginary part of measurement error.

Considering measured aliased voxel in Eq. 2.4 across the N_c coils for N_s aliased slices with N_α time-points in the fMRI time series, Eq. 2.4 can be expressed as:

$$a = X_A \beta + \varepsilon. \tag{2.5}$$

N_α denotes the number of sequential time-points of the Hadamard encoded pattern, and it is an integer between 1 and N_s. Therefore, the net acceleration of the fMRI time series acquisition is defined as $A = N_s/N_\alpha$. In Eq. 2.5, the dimension of a is $2N_cN_\alpha \times 1$ including the real and imaginary components. The measurement error, ε, has the same dimension as a with the mean $E(\varepsilon) = 0$ and covariance $cov(\varepsilon) = \sigma^2 I_{2N_cN_\alpha}$. The dimension of the aliasing matrix, X_A, is $2N_cN_\alpha \times 2N_sN_r$, where N_r is an indicator of the number of matrix rotation operations. In this study, we generally assign $N_r = N_s$ to improve the computational efficiency. The true voxel value, β, has

the dimension of $2N_sN_r \times 1$, including the real and imaginary value for each voxel. For the δth Hadamard aliasing pattern and γth matrix rotating operation, the aliasing matrix $(X_A)_{\gamma,\delta}$ across N_c coils is defined as:

$$(X_A)_{\gamma,\delta} = \left[H_{\delta,1} R_{\gamma,1} \begin{pmatrix} S_{1,1} \\ \vdots \\ S_{N_c,1} \end{pmatrix}, \dots, H_{\delta,N_s} R_{\gamma,N_s} \begin{pmatrix} S_{1,N_s} \\ \vdots \\ S_{N_c,N_s} \end{pmatrix} \right]. \tag{2.6}$$

$R_{\gamma,z}$ is the matrix rotate operator which should work on coil sensitivity maps for each slice, and it is not the matrix multiplication. Across the N_α excitations, the aliasing matrix X_A can be written as:

$$X_A = \begin{bmatrix} (X_A)_1 \\ \vdots \\ (X_A)_{N_\alpha} \end{bmatrix}. \tag{2.7}$$

To separate the aliased images and estimate the voxel value for each slice, the least square estimation method is used. The estimated separate voxel value, $\hat{\beta}$, can be calculated by:

$$\hat{\beta} = (X_A' X_A)^{-1} X_A' a. \tag{2.8}$$

In general, the determinant of X_A is close to zero, $\det(X_A) \approx 0$, which leads to a failure to calculate the inverse of $X_A' X_A$. Thus, a bootstrap sampling method incorporating with artificial aliasing of reference calibration images technique are combined with the mSPECS-CAIPI method. These two techniques can eliminate the inter-slice signal leakage artifacts by introducing a regularizer in the least square estimation function and making the aliasing matrix to be full rank for the inverse. More details will be shown in the following section. In Figure 2.5, the top picture illustrates the data-acquiring process of the mSPECS technique (without any image shifts), the middle picture illustrates the data-acquiring process of the mSPECS-CAIPIRINHA technique, and the bottom picture illustrates the data-acquiring process of the mSPECS-CAIPIVAT technique.

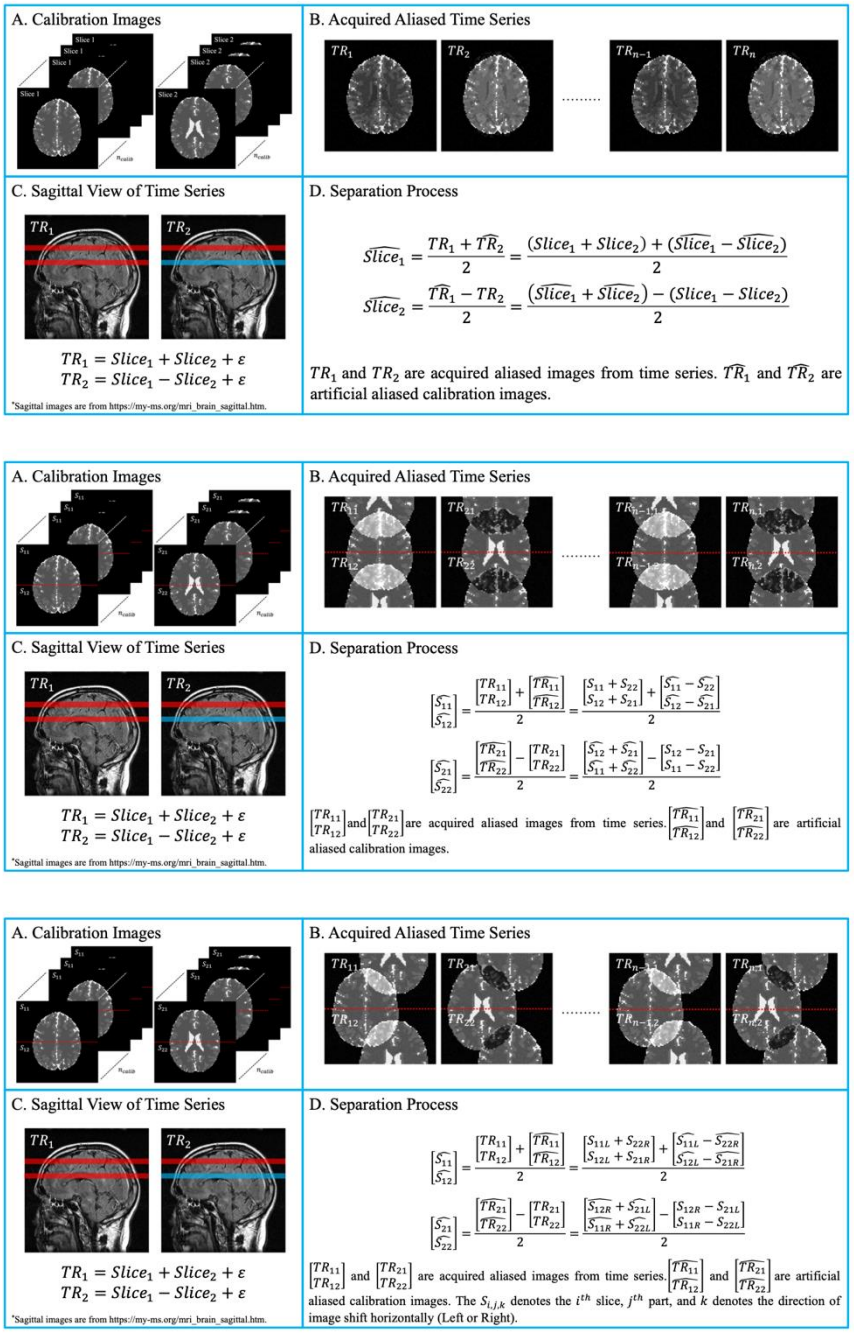

Figure 2.5. The top picture illustrates the data-acquiring process of the mSPECS techinque (without any image shifts), the middle picture illustrates the data-acquiring process of the mSPECS-CAIPIRINHA technique, and the bottom pictures illustrates the data-acquiring process of the mSPECS-CAIPIVAT technique.

2.2 The Bootstrap Sampling and Artificial Aliasing of Calibration Images

In the previous simultaneous multi-slice (SMS) study, bootstrap sampling and artificial aliasing of calibration reference image techniques have been proven as powerful tools to support the separation

and reconstruction process of aliased images. By increasing the size of the aliasing matrix and adding a regularizer into the least square estimation function, the correlation induced by the separation process will decrease and the slice-to-slice signal leakage will be eliminated. In the fMRI time series, for each excitation, N_s bootstrap sampled coil slice images will be randomly chosen from fully sampled calibration reference images. The mean calibration images will be calculated for each slice. Then the mean calibration images will be artificially aliased, and this process will be repeated for each TR.

Given a single TR, the calibration images will have the same shift pattern as acquired images, thus, the total number of different combinations for different voxels should be N_S, which is equal to the rank of the chosen Hadamard matrix. After removing the combination of the acquired aliasing pattern from the full voxel combination pattern, $N_S - 1$ different combinations remain. Therefore, for a single excitation, a voxel across N_S slices, measured through N_c coils, v, can be represented as a vector with the dimension of $2N_SN_c(N_S - 1) \times 1$ corresponding to the remain combinations without the acquired aliasing combination. The mean bootstrap sampled voxel, $\bar{v}$, is with the same dimension as v for each time point. The artificial aliasing calibration images, ν, across N_S slices measured through N_c coils at N_α sequential time point can be expressed as:

$$\nu = C\bar{v} = C_A\mu + C\eta. \tag{2.9}$$

In the Eq. 2.9, ν is a $2N_SN_c(N_S - 1) \times 1$ vector includes real and imaginary components for the artificial aliasing voxel values. The mean calibration images vector, $\bar{v}$, contains real and imaginary parts for the bootstrap sampled mean voxel value with the same dimension as ν. The dimension of the measurement error vector, η, is the same size as the vector ν. The mean of the measurement error for the calibration images is $E(\eta) = 0$, and the covariance is $cov(C\eta) = \sigma^2 I_{2N_SN_c(N_S-1)}$, where $I_{2N_SN_c(N_S-1)}$ is the identity matrix. There is no correlation between the real and imaginary components of the calibration images because they do not change. The true voxel value vector, μ, constructed with the real and imaginary components of the calibration voxel with the dimension $2N_S \times 1$. The artificial aliasing matrix, C_A, is following the same aliasing rules as acquired images do, rotating by the matrix rotation operation and multiplying the Hadamard encoding aliasing coefficients. Due to the combination of acquired aliasing voxel removed from the full combinations, the dimension of the artificial aliasing matrix should be $2N_SN_c(N_S - 1) \times 2N_S$. Same as the assumption in the acquired aliasing images, we assign $N_r = N_S$ to improve the computational efficiency. For example, considering a situation with $N_S = 4$, and $N_r = 4$, for each time point, $N_S - 1 = 3$ combinations should be applied with the calibration images. Thus, for a given excitation, the δth Hadamard aliasing pattern and γth matrix rotating operation, the aliasing matrix $(C_A)_{\gamma,\delta}$ across N_c coils can be written as:

$$(C_A)_{\gamma,\delta} = \left[\overline{H_{\delta,1}R_{\gamma,1}}\begin{pmatrix} S_{1,1} \\ \vdots \\ S_{N_c,1} \end{pmatrix}, \dots, \overline{H_{\delta,N_S}R_{\gamma,N_S}}\begin{pmatrix} S_{1,N_S} \\ \vdots \\ S_{N_c,N_S} \end{pmatrix}\right]. \tag{2.10}$$

The notation $\overline{HR}$ denotes the remaining combination for the Hadamard encoding aliasing pattern with the matrix rotation pattern after removing the combination of the acquired aliasing pattern. Incorporating N_α sequential time points, the artificial aliasing matrix, C_A, can be written as:

$$C_A = \begin{bmatrix} (C_A)_1 \\ \vdots \\ (C_A)_{N_\alpha} \end{bmatrix}. \tag{2.11}$$

2.3 The Statistical Separation Process

To separate the aliased voxel, according to mSPECS-CAIPI approach, we combine the Eq. 2.5 and Eq. 2.9 together, which will generate:

$$y = \begin{bmatrix} a \\ \nu \end{bmatrix} = \begin{bmatrix} X_A\beta \\ C_A\mu \end{bmatrix} + \begin{bmatrix} \varepsilon \\ C\eta \end{bmatrix}. \tag{2.12}$$

The dimensions for each parameter in the equation are discussed in detail in the previous sections. The least squares estimation function is incorporated with the mSPECS-CAIPI method, which will lead us to:

$$\hat{\beta} = (X_A' X_A + C_A' C_A)^{-1}(X_A' a + C_A' v). \quad (2.13)$$

$C_A' C_A$ works as the regularizer for matrix inverse to improve the condition of the equation. The expectation value of the estimation images is:

$$E(\hat{\beta}) = (X_A' X_A + C_A' C_A)^{-1}(X_A' E(a) + C_A' E(v)). \quad (2.14)$$

Based on the previous section, the covariance for the acquired aliasing measurement error is $cov(\varepsilon) = \sigma^2 I_{2N_c N_\alpha}$, and the covariance for the artificial aliasing measurement error is $cov(C\eta) = \sigma^2 I_{2N_S N_c (N_S N_r - 1)}$, the covariance for vector, y, consisting of acquired aliasing voxel value and the artificial aliasing voxel value is:

$$cov(y) = \begin{bmatrix} \sigma^2 I_{2N_c N_\alpha} & 0 \\ 0 & \tau^2 I_{2N_S N_c (N_S N_r - 1)} \end{bmatrix}. \quad (2.15)$$

Without the support of the bootstrapping technique, there will be no variation in the artificial aliasing calibration images, i.e. same calibration reference images will be artificially aliased for each TR, which will lead to $\tau^2 = 0$. The correlation induced by the separation process will increase and the slice-to-slice signal leakage artifacts will display. With the help of the bootstrap sampling approach, $\tau^2 = \sigma^2$, such that the covariance of $\hat{\beta}$ is:

$$cov(\hat{\beta}) = \sigma^2 (X_A' X_A + C_A' C_A)^{-1}. \quad (2.16)$$

Therefore, the correlation induced by the unaliasing process is minimized, and the inter-slice signal leakage artifacts are eliminated.

3. Materials

3.1 The simulated fMRI data

The mSPECS-CAIPI model will be applied to simulated fMRI data, and the results will be compared with the mSPECS method. The resting state simulated fMRI data and the task activation simulated fMRI data will be investigated separately. The resting state simulated fMRI data experiment includes 640 TRs, with the first 40 TRs used as calibration images. The experiment is performed with the number of coils $N_c = 32$, and the total number of images $N_s = 8$. In order to investigate and compare the reconstructed images with different through-plane acceleration, we will perform resting state simulated experiments with $TPA = 2$, $TPA = 4$ and $TPA = 8$. Incorporating different through-plane acceleration factors, images will be put into different packets. When $TPA = 2$, there are four packets with packet 1: slice 1 and slice 5, packet 2: slice 2 and slice 6, packet 3: slice 3 and slice 7, and packet 4: slice 4 and slice 8. When $TPA = 4$, two packets with the odd number of slices in one packet and the even number of slices in the other packet will be implemented. When $TPA = 8$, all slices are put into one packet. The task activation simulated fMRI data experiment also includes 640 TRs, with the first 40 TRs used as calibration images. The size of the simulated task activation block is 6×6, and manually added to the simulated fMRI data with 15 TRs on and 15 TRs off, cycling 20 times. The same number of coils $N_c = 32$, and the same images $N_s = 8$ as the resting state simulated experiment will be used in the model. The same through-plane acceleration factors will be chosen to implement. All experiments will be performed on Matlab program software. Figure 3.1 is the true noiseless magnitude of the $N_s = 8$ slices of sagittal images. Figure 3.2 is the magnitude of the $N_c = 32$ simulated coils sensitivity information mimics the real 32-channel head receiver coils. In the simulated coils, we assumed the first 12 coils are on the top portion of the head receiver coil, and the rest 20 coils are on the bottom portion of the head receiver coil.

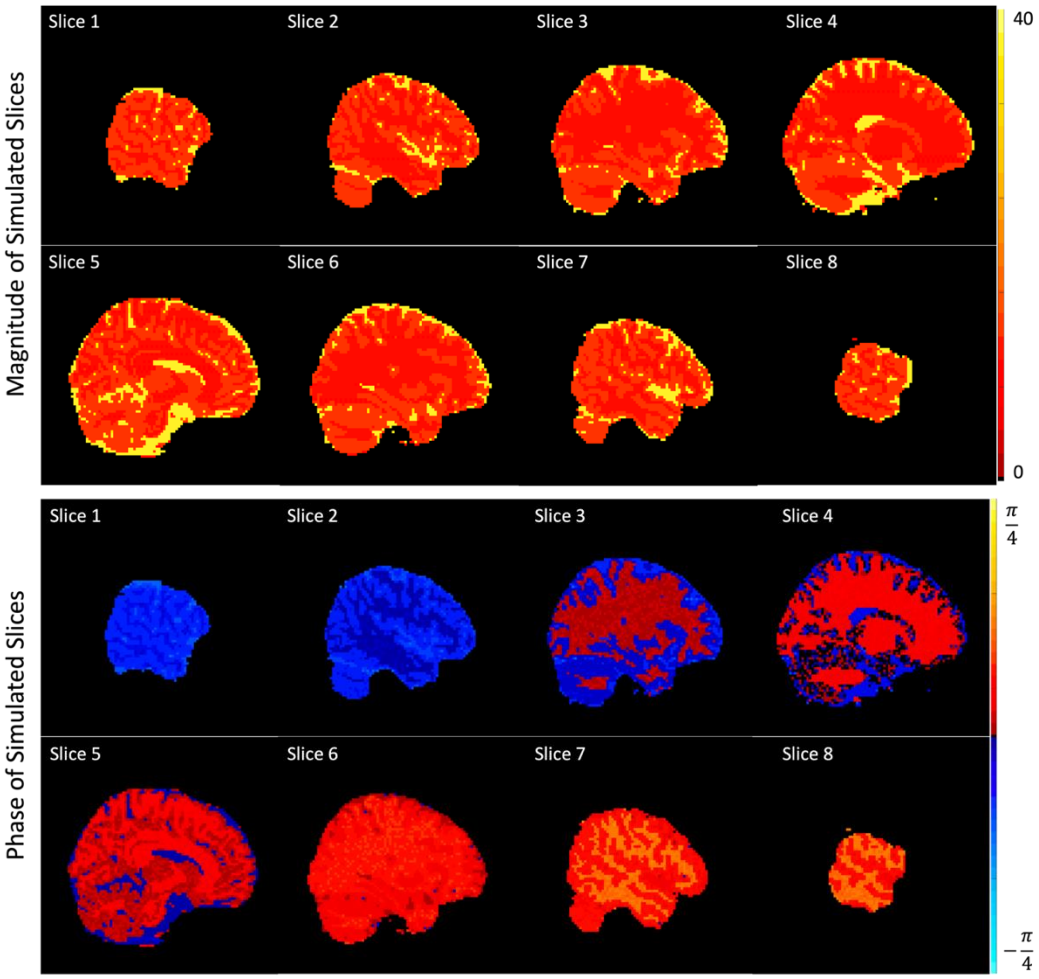

Figure 3.1 The true noiseless magnitude and phase of the simulated sagittal images.

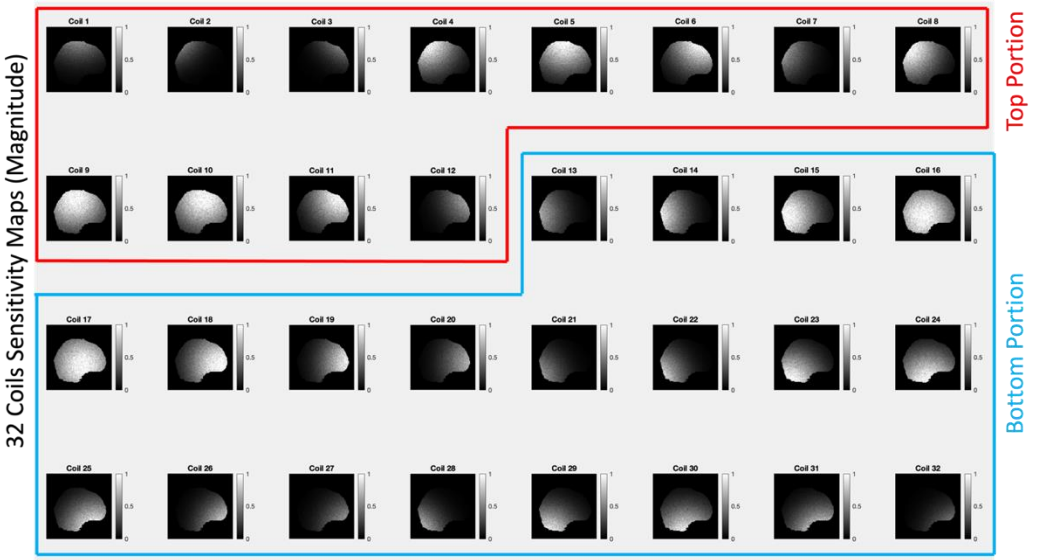

Figure 3.2 The magnitude of the 32-channel coils, with the first 12 coils on the top portion of the head receiver coil and the rest 20 coils on the bottom portion of the head receiver coil.

4. Simulated Results

According to the methodology of the mSPECS-CAIPI model, we performed the simulated experiment with different through-plane acceleration factor $TPA = 2$, $TPA = 4$, and $TPA = 8$, and compared the results with the same acceleration factors from the mSPECS model and standard SENSE models. Figure 4.1 is the temporal mean magnitude and temporal mean phase value of the reconstructed images from standard SENSE, mSPECS, mSPECS-CAIPIRINHA, and mSPECS-CAIPIVAT models with through-plane acceleration factor $TPA = 8$. From Figure 4.1, we can see that there is a strong signal leakage in the reconstructed images from the standard SENSE model. Compared with magnitude and phase images from mSPECS, mSPECS-CAIPIRINHA and mSPECS-CAIPIVAT model, signal from other slides appears on the magnitude and phase images of SENSE model. The mSPECS, mSPECS-CAIPIRINHA and mSPECS-CAIPIVAT model provide us more accurate reconstructed images compared with the true magnitude and phase. The *SNR* value and *g*-factor value are also compared among four models. Based on the definition of the temporal signal-to-noise ratio, $SNR = \frac{\bar{S}}{\sigma_N}$, where $\bar{S}$ is the mean magnitude value in the time series, and σ_N is the standard deviation of the magnitude of the noise. The signal-to-noise ratio also can be expressed as $SNR = \frac{\beta_0}{\sigma_N}$, where β_0 is the baseline signal, and σ_N is the standard deviation of the magnitude of the noise. According to the definition of *SNR* in section 2.1.1, the *g*-factor can be calculated as $g_{accelerate} = \sqrt{N_s}\frac{SNR_{full}}{SNR_{accelerate}\sqrt{R}}$, where SNR_{full} is the SNR map from model without acceleration technique, and R indicates the in-place acceleration factor, which in this case $R = 1$. Thus, the *g*-factor also indicates the noise amplification level of the model. Figure 4.2 is the temporal *SNR* map and *g*-factor map for standard SENSE, mSPECS, mSPECS-CAIPIRINHA and mSPECS-CAIPIVAT models. From Figure 4.2, the standard SENSE model provides us low *SNR* map and high *g*-factor penalty. Although we can access a good *SNR* map and *g*-factor map from the mSPECS model, the mSPECS-CAIPIRINHA and mSPECS-CAIPIVAT models provide us a better *SNR* map and *g*-factor map with much higher *SNR* value and lower *g*-factor penalty.

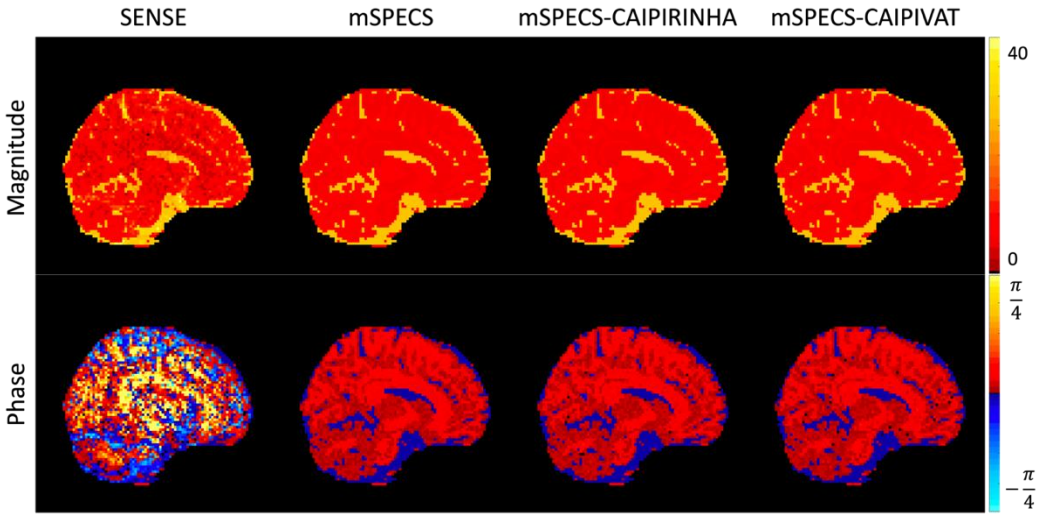

Figure 4.1 The temporal mean magnitude and temporal mean phase value of reconstructed images from standard SENSE, mSPECS, mSPECS-CAIPIRINHA, and mSPECS-CAIPIVAT models with through-plane acceleration factor $TPA = 8$.

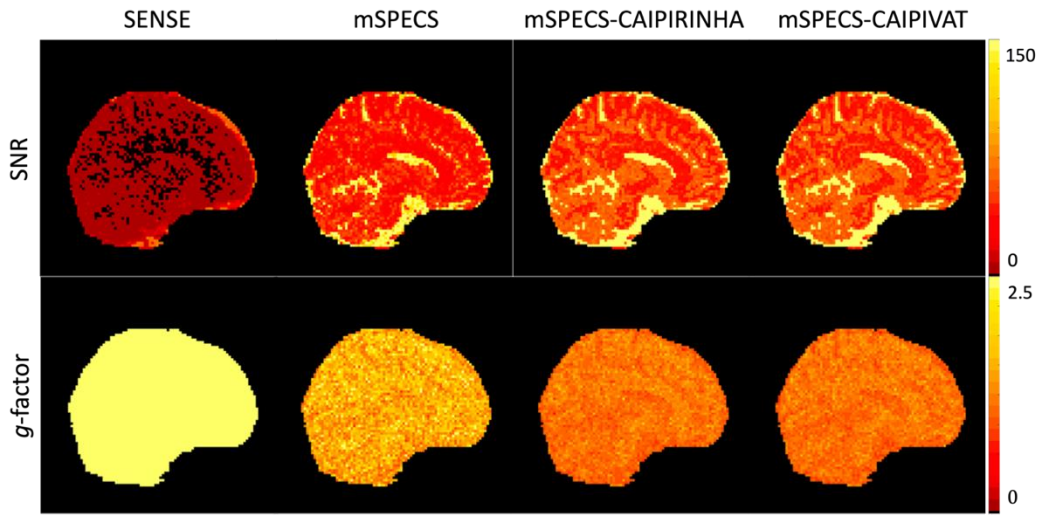

Figure 4.2 The temporal SNR map and g-factor map from standard SENSE, mSPECS, mSPECS-CAIPIRINHA and mSPECS-CAIPIVAT models with through-plane acceleration factor $TPA = 8$.

We also applied the standard SENSE, mSPECS, mSPECS-CAIPIRINHA and mSPECS-CAIPIVAT models to the task simulated data with different through-plane acceleration factors. The *CNR* value and the activation detection map are also investigated. Given the contrast-to-noise ratio, $CNR = \frac{\beta_1}{\sigma_N}$, where β_1 is the activation signal, and σ_N is the standard deviation of the magnitude of the noise. The activation detection is based on a complex way to compute fMRI activation (Rowe and Logan, 2004). Figure 4.3 is the *CNR* value and the activation detection map for SENSE, mSPECS, mSPECS-CAIPIRINHA and mSPECS-CAIPIVAT model. The average *CNR* value inside of the ROI is increasing from SENSE model to mSPECS-CAIPI model, from 0.28 to 0.88. And the average activation value inside of the ROI is also increasing from SENSE model to mSPECS-CAIPI model, from 0.92 to 5.44. Based on the simulated results from resting state data and task data, we can conclude that the mSPECS-CAIPI model can provide us a high-quality, high-resolution reconstructed images compared with mSPECS and SENSE model. The mSPECS-CAIPI model preforms better capturing the task activation block, whereas SENSE model cannot capture any activation block inside of the brain image.

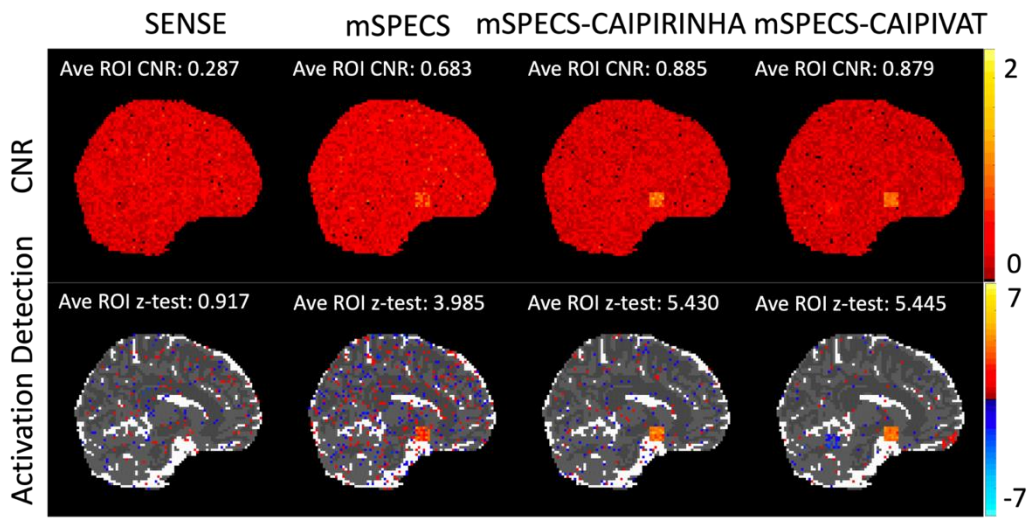

Figure 4.3 The *CNR* map and activation detection map for SENSE, mSPECS, mSPECS-CAIPIRINHA and mSPECS-CAIPIVAT models with through-plane acceleration factor $TPA = 8$.

5. Conclusion

In this paper, we introduce a novel SMS technique called mSPECS-CAIPI model, which incorporates unique imaging shift methods, CAIPIRINHA and CAIPIVAT. We also incorporate the Hadamard phase encoding technique to increase the size of the aliasing matrix. Bootstrapping and artificial aliasing of calibration images are also included in our model. We applied our model to the resting state simulated data and the task simulated data and compared the reconstructed results with previous models, SENSE and mSPECS. We can conclude that compared with the previous model, our model can reduce the scan time by incorporating the subsampling method, but at the same time, still can generate high-quality and high-resolution reconstructed images. Also, our model can capture more activation information from the functional dataset.

Acknowledgements

The authors thank the Wehr Foundation at this research funded by the Computational Sciences Summer Research Fellowship (CSSRF) at Marquette University in the Department of Mathematical and Statistical Sciences.

Reference

Barth M, Breuer F, Koopmans PJ, Norris DG, Poser BA. *Simultaneous multislice (SMS) imaging techniques.* Magn Reson Med. 2016 Jan;75(1):63-81.

Felix A Breuer, Martin Blaimer, Robin M Heidemann, Matthias F Mueller, Mark A Griswold, Peter M Jakob. *Controlled aliasing in parallel imaging results in higher acceleration (CAIPIRINHA) for multi-slice imaging.* Magn Reson Med 2005 Mar;53(3):684-91.

Glover GH. *Overview of functional magnetic resonance imaging.* Neurosurg Clin N Am. 2011 Apr;22(2):133-9, vii.

Griswold MA, Jamob PM, Heidemann RM, Nikkka M, Jellus V, Wang J, Kiefer B, Haase A. *Generalized autocalibrating partially parallel acquisition (GRAPPA).* Mag. Res. Med, 47:1202–1210, 2002.

Jungmann PM, Ganter C, Schaeffeler CJ, Bauer JS, Baum T, Meier R, Nittka M, Pohlig F, Rechl H, von Eisenhart-Rothe R, Rummeny EJ, Woertler K. *View-Angle Tilting and Slice-Encoding Metal Artifact Correction for Artifact Reduction in MRI: Experimental Sequence*

Optimization for Orthopaedic Tumor Endoprostheses and Clinical Application. PLoS One. 2015 Apr 24;10(4):e0124922.

Kociuba CM. *A Fourier description of covariance, and separation of simultaneously encoded slices with in-plane acceleration in fMRI*. Ph.D. Dissertation. Marquette University, Milwaukee, Wisconsin, USA. 2016.

Min-Oh Kim, Taehwa Hong, Dong-Hyun Kim. *Multislice CAIPIRINHA Using View Angle Tilting Technique (CAIPIVAT).* Tomography. 2016 Mar; 2(1): 43-48.

Min-Oh Kim, Sang-Young Zho, Dong-Hyun Kim. *3D imaging using magnetic resonanace tomosynthesis (MRT) technique.* Med. Phts. 39 (8), August 2012: 4733-4741.

Ogawa S, Lee TM, Kay AR, Tank DW. *Brain magnetic resonance imaging with contrast dependent on blood oxygenation.* Proc Natl Acad Sci U S A. 1990 Dec;87(24):9868-72.

Preibisch C, Castrillón G. JG, Bührer M, Riedl V (2015) *Evaluation of Multiband EPI Acquisitions for Resting State fMRI*. PLoS ONE 10(9): e0136961.

Pruessmann KP, Weiger M, Scheidegger MB, Boesiger P. *SENSE: Sensitivity Encoding for Fast MRI.* Mag. Res. Med, 42:952–962, 1999.

Rowe DB, Bruce IP, Nencka AS, Hyde JS, Kociuba MC. *Separation of parallel encoded complex-valued slices (SPECS) from a signal complex-valued aliased coil image.* Magn Reson Imaging. 2016 Apr;34(3):359-69.

Rowe DB, Logan BR. *A complex way to compute fMRI activation.* Neuroimage. 2004 Nov;23(3):1078-92.

Setsompop K, Gagoski BA, Polimeni JR, Witzel T, Wedeen VJ, Wald LL. *Blipped-controlled aliasing in parallel imaging (blipped-CAIPI) for simultaneous multi-slice EPI with reduced g-factor penalty.* Magn Reson Med. 2012 May;67(5): 1210-1224.

Sodickson DK, Manning WJ. *Simultaneous acquisition of spatial harmonics (SMASH): fast imaging with radiofrequency coil arrays.* Magn Reson Med. 1997 Oct;38(4):591-603.

Souza SP, Szumowski J, Dumoulin CL, Plewes DP, Glover G. *SIMA - simultaneous multislice acquisition of MR images by Hadamard-encoded excitation.* J Comput Assist Tomogr 1988;12:1026–1030.

Welvaert M, Rosseel Y (2013). *On the Definition of Signal-To-Noise Ratio and Contrast-To-Noise Ratio for fMRI Data.* PloS ONE 8(11): e77089.